Electrical properties of frustrated twisted grain boundary phases of liquid crystalline materials

M. B. Pandey[1] *AND Ravindra Dhar*[1,2]

Abstract | An overview of characteristics physical properties of twisted grain boundary (TGB) phases shown by some of the chiral liquid crystalline materials is given. After a brief discussion of various liquid crystalline phases, structure of various types of TGB phases, their general behaviour along with optical textures and some other characteristics have been discussed. Finally, details about dielectric behaviour of TGB phases with static and dynamic measuring electric field are reported and discussed.

1. Introduction

Liquid crystals constitute a fascinating phase of condensed matter in which the molecules are partially ordered and hence the material shows crystalline anisotropy and also the molecules are not perfectly rigid with respect to each other, hence the material shows some of the liquid properties viz. flow with large viscosity[1–4]. As the name indicates these material possesses the properties similar to those of a liquid and simultaneously exhibits anisotropic tensorial properties such as electrical conductivity, dielectric anisotropy, optical birefringence etc. similar to those of ordered crystalline solids. The duality in the physical properties of this state of matter is the reason behind the name Liquid Crystal. Liquid crystal phases have been first discovered in 1888 by F. Reinitzer[5]. Till now a large number of organic compounds are known, which exhibit this fascinating intermediate phase of matter. The studies of liquid crystals get enormous consideration not only because of its peculiar nature but also due to its technological importance.

Liquid crystals are classified mainly into two categories[1–4]. One is thermotropics in which different type of liquid crystal phases (called mesophases) are achieved by temperature variation of the material and the temperature at which one mesophase goes into other mesophase is called transition temperature. Second category of liquid crystal is of lyotropics in which mesophases occur by changing the concentration of some appropriate solvents. Lyotropics are found mainly in biological systems. Thermotropics have now become an integral part of present high tech device and hence they are of main concern to physicist and technologist.

Mesophase of the thermotropic liquid crystals are broadly classified into two categories[1–4] viz. nematics (N) and smectics (Sm) phases. These mesophases differ primarily in the manner in which the molecules order themselves relative to their neighbours. The least ordered liquid crystal phase structure is nematic. Most of the substances exhibiting this phase consist of rod-like molecules in which the long axes of the molecules are aligned along a common axis called director ($\hat{n}$). Such type of ordering is known as orientational ordering. In the smectic phase of liquid crystals, the molecules are packed in layers, side by side within layer, but end to end from one layer to another. Within these constraints the molecules can be packed

[1]*Department of Physics, University of Allahabad, Allahabad 211 002, India*
[2]*Department of Physics, Ewing Christian College, University of Allahabad, Allahabad 211 003, India*
dr_ravindra_dhar@hotmail.com

Keywords: TGB phases, chirality, smectic slabs, phase diagram, optical texture, Dielectric permittivity, Relaxation modes.

Figure 1: Schematic representation of TGBA (originally SmA*) phase proposed by Renn and Lubensky[8]. Here blocks of SmA layers of spacing d are separated by regularly spaced twist grain boundaries separated by a distance l_b. The distance between screw dislocations within a grain boundary is l_d. The normal to the smectic planes of consecutive blocks separated by a grain boundary changes by angle $\Delta\chi(=d/l_d)$ while moving along helix axis ($\hat{P}$).Distance corresponding to rotation of the blocks by angle π corresponds to half of the pitch P.

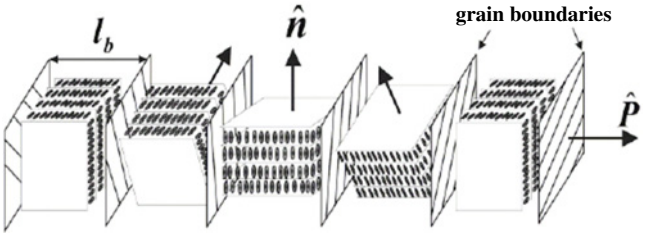

in several different manners and hence giving rise to several classes of smectic structures such as smectic A, B, C...K which manifest them in different characteristic texture when observed under a polarizing microscope[6]. In some smectic phases such as SmA, SmB, SmD and SmE, the long axes of the molecules are essentially normal to the layer planes whereas in other phases such as SmC, SmI, SmG, SmF, SmJ and SmK, they are tilted with respect to the layer normal with a tilt angle θ. These smectic phases differ from each other in their molecular packing arrangement as revealed by X-ray diffraction[1].

Cholesteric (N^*) phase is the chiral analog of nematic phase and is observed when molecules of the liquid crystalline material have chirality or chiral molecules (mesogenic or non mesogenic) are added to the nematic phase. In the chiral nematic phase director ($\hat{n}$) rotates continuously due to molecular chirality while moving along an axis (called helix axis) normal to the director. Length on the helix axis corresponding to the rotation of the director by angle π corresponds to half of the pitch.

In 1972, de Gennes pointed out analogy between the smectic-nematic phase transition in liquid crystals and the super conduction-normal conduction transition in metals[6,7]. Due to this analogy, he predicted that the regular defect structure should occur in smectic phases close to the Sm-N transition when a twist or bend deformation is exerted on the director field of the Sm phase. This defect structure is analog of the mixed state in type II super conductors, which exhibits a lattice of magnetic flux lines. In 1988, Renn and Lubensky extended the theory of Sm-N transition to chiral systems and pointed out that intrinsic twist of N* phase can act as an external field just like the mechanical deformation considered by de Gennes, thereby leading to "twisted SmA (SmA*)" structure in the chiral systems[8]. This "twisted SmA (SmA*)" structure predicted by Renn and Lubensky is now called twisted grain boundary (TGB) A phase. Structure of TGBA phase predicted by Renn and Lubensky[1] is shown in Figure 1.

TGBA phase shown in Figure 1 consists of smectic slabs, separated by defect walls (grain boundaries) consisting of defect lines (twist dislocations). In the slabs, molecules are arranged in layers with their director normal to the smectic layers. Neighbouring slabs (and hence molecular director in the slabs) are twisted with respect to each other by angle $\Delta\chi$, thereby forming helical structure with the helix axis ($\hat{P}$) normal to the molecular director[8]. A length along helical axis corresponding to the twist of smectic slabs (director) by angle π is the half of the pitch of the TGB helix. Length of the smectic slabs (l_b), distance between defect lines (l_d) and pitch (P) are related by the equation

$$p = \Delta\chi/2\pi = l_b/P = 2\sin^{-1}(d/2l_d)/2\pi \quad (1)$$

where d is the layer spacing and p is a number. If p is irrational, the structure is incommensurate i.e. there is no periodicity of the orientation of the slabs along the pitch axis, however, if p is rational, the system is commensurate and has n-fold screw axis.

In the temperature range close to $T_{\mathrm{SmA-N}}$, phase transition from SmA-N phase can be described by Landau-Gennes theory[2,9,10]. The free energy density (g_{lc}) is expanded in the power series of order parameter (ψ) as

$$g_{lc} = \frac{1}{2}\left[\alpha\psi^2 + \frac{1}{2}\beta\psi^4 + \frac{1}{3}\gamma\psi^6\right] \quad (2)$$

where $\alpha = a(T - T_{SmA-N})$ with $a > 0$. Depending on the values of β and γ, a transition may be of the first order ($\beta < 0 < \gamma$), second order ($\beta > 0$, $\gamma = 0$)

or tricritical ($\beta = 0, \gamma > 0$). Order parameter ψ is nonzero in Sm phase but vanishes in N phase. Renn and Lubensky[8] extended the theory of the Sm-N transition to chiral systems and extended equation 2 as

$$g_{lc} = g_0 + \frac{1}{2}\left[\alpha\psi^2 + \frac{1}{2}\beta\psi^4 + C\{(\nabla - iQn)\psi\}^2\right] + \frac{1}{2}[K_{11}(\vec{\nabla}.\hat{n})^2 + K_{22}\{(\hat{n}.\vec{\nabla}x\hat{n}) + q_0\}^2 + K_{33}\{\hat{n}x(\vec{\nabla}x\hat{n})\}^2 - K_{22}q_0^2] \quad (3)$$

where K_{11}, K_{22}, and K_{33} are respectively, the splay, twist and bend elastic constants. This equation is very similar to the Landau-Ginzburg free-energy density of superconductors given as[11–14]

$$g_{sc} = g_n + \frac{1}{2}\left[\alpha\psi^2 + \frac{1}{2}\beta\psi^4 + (2m_e)^{-1}\{(-ih\vec{\nabla} - 2e\vec{A})\psi\}^2] + (2\mu)^{-1}(\vec{\nabla}x\vec{A})^2 - H_0(\vec{\nabla}x\vec{A}) + \frac{1}{2}\mu_0 H_0^2\right] \quad (4)$$

ψ of equation 4 corresponds to the wave function describing the Bose condensate of Cooper pairs and $\vec{A}$ is the magnetic vector potential. The analogy between liquid crystals and superconductors after the work of de Gennes[6,7] and Renn and Lubensky is given in table 1[8].

2. Experimental observation of TGBA phase

SmA* (now TGBA) phase predicted by Renn and Lubensky[8] was first observed by Goodby *et al.* in 1989 as an independent work on the highly chiral homologous series of ferroelectric liquid crystal material R- and S-1-methylheptyl 4′-[(4″-n-alkoxyphenyl)propionoyloxy]-biphenyl-4-carboxylates (nP1M7), with n=13, 14 and 15[15]. X-ray studies on non-aligned samples together with textural studies indicated that the SmA* simultaneously exhibited both smectic layering and cholesteric like textures and therefore Goodby *et al.* proposed that the SmA* might, in fact be the TGB (A) phase. This identification has since been confirmed by a high resolution X-ray study on aligned samples by Srajer *et al.*[16]. Almost simultaneously this phase was observed by Lavrentovich *et al.* (1990) in the binary mixtures of cholesteryl nonanoate and nonyloxybenzoic acid[17]. Srivastava *et al.*, latter reported detailed thermodynamic and electrical studies on this mixture[18,19]. Existence of additional (TGBA) phase between N* and SmA phase was confirmed by dielectric studies as well on the aligned samples[19].

Re-entrant phenomenon of TGBA phase along with re-entrant of cholesteric phase has also been reported in mixtures[20]. Shankar Rao *et al.* reported re-entrant TGBA phase in a cholesterol based non-symmetrical dimer, namely cholesteryl 6-[4-(4-hexyloxy phenylethynyl) phenoxy] hexanoate[21]. Pressure induced TGBA phase in between N* and SmA phases has also been reported[22]. There are several pure[23–31] as well as mixed systems[32–39] that have shown TGBA phase till date. In fact binary system of cholesteryl benzoate (ChB) and di-heptyloxyazoxybenzene (HOAB) has shown largest temperature range (>40 °C) of TGBA phase[32,33]. DSC thermogram of the binary mixture of ChB and HOAB having wide temperature range TGBA phase is shown in Figure 2. Following studies on the large number of systems showing TGB and other frustrated phases, Goodby *et al.* have described in details about the molecular systems required to produce TGB phases[40–42]. In general, high chirality and weak layered structure are the pre conditions for the occurrence of the TGB phases. It is important to note that as the smectic slabs in the proposed structure (Figure 1) and in experimental materials as well were SmA hence TGB phase was given specific name TGBA.

The first clear and convincing experimental proof of TGBA structure came after the freeze-fracture transmission electron microscopy (TEM) of 14P1M7 by Ihn *et al.*[43]. Optical diffraction from the TEM showed that the layer spacing (d) in TGBA phase of 14P1M7 is approximately 4.1 nm and that the rotation of blocks of Sm layers along the helix axis occurs in the discrete step of roughly 17° between adjacent blocks ($= \Delta\chi$). Pitch of the helix (P) has been found to be 500–600 nm, which falls in the wavelength region of the visible light and hence TGBA phase shows selective reflection for visible light. TEM data obtained by Ihn *et al.* indicated that in TGBA phase, screw dislocations are 14–15 nm apart ($= l_d$) whereas grain boundaries are about 24–28 nm apart ($= l_b$) [43]. Several other structural studies have been reported confirming the nano structure of TGB phase[44,45]. Navailles *et al.*, have reported X-ray scattering experiments on TGBA phase of the 10th homolog of nF2BTF01M7[45]. Figure 3 shows X-ray scattering pattern obtained for TGBA phase. This pattern exhibits 46 equispaced spots along the ring and indicates commensurate structure of TGBA phase. Navailles *et al.* reported $\Delta\chi = 7.8^0$, $l_b = 20.6$ nm and $l_d = 27.8$ nm[45]. Therefore l_b/l_d (=0.74) has been found to be close to 1 as theoretically predicted by Renn and Lubensky[8]. Bluestein *et al.*[46] have latter calculated the value of $l_b/l_d = 0.95$, which is more close to the experimental data. However, Boulder group

Table 1:

Superconductors	Liquid Crystals
Cooper pair amplitude, ψ	density wave amplitude, ψ
Vector potential, $\vec{A}$	nematic director, $\hat{n}$
Magnetic induction, $\vec{B} = \vec{\nabla} x \vec{A}$	twist, $k_0 = \hat{n}.(\vec{\nabla} x \hat{n})$
Normal metal	Nematic phase
Normal metal in magnetic field	Chiral Nematic/Cholesteric (N^*) phase
Magnetic field, H	Chirality field, $K_{22} k_0$
Meissner phase	Smectic A phase
Meissner effect	Twist expulsion
Inverse magnetic permeability, μ^{-1}	Twist elastic coefficient, K_{22}
London penetration depth, λ	Twist penetration depth, λ_2
Superconducting coherence length, ξ	Smectic correlation length, ξ
Ginzburg parameter, $\kappa =$ $(\beta/2\mu)^{1/2} m_e \hbar^{-1} e^{-1}$	Twist Ginzburg parameter, $\kappa =$ $(K_{22}\beta/2)^{1/2} C^{-1} Q_0^{-1}$
Inverse mass of the Cooper pairs, $\hbar^2/2m_e$	Smectic elastic constant, C
Magnetic flux quantum, $\varphi_0 = h/2e$	Layer spacing, d
Magnetic energy	Frank-Oseen elastic energy
Charge on the Cooper pairs, $2e/\hbar$	Wave vector, $Q_0 = 2\pi/d$
Vortex (magnetic flux tube)	Screw dislocation
Abrikosov flux lattice	Twisted-grain-boundary (TGB) phase

Figure 2: DSC thermogram for the binary mixture of ChB and HOAB (in mole ratio of 0.25 and 0.75) at the scanning rate of 10 °C/min[104] (after the work of Kuczynski and Stegemeyer[32]). Temperature range of TGBA phase shows super cooling effect and exists for more than 40 °C in cooling cycle. Melting and crystallization peaks are not shown in order to increase the visibility of smaller peaks.

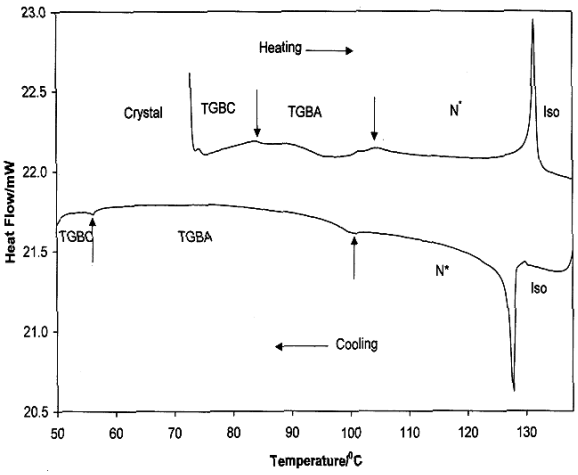

have studied different kind of materials showing TGBA phase in wide temperature range[47]. They have found that a common feature between them is 'Giant' smectic blocks of planar layers of thickness l_b exceptionally lying between 200 and 2000 nm whereas $\Delta\Psi$ lying between 60 and 90°. Zhang et al have reported deuterium NMR study on TGBA phase of 4-[4 ℓ-(1-methyl heptyloxy)] biphenyl 4-(10-undecenyloxy) benzoate (11EB1M7)[48]. This study shows the arrangement of helical structures of TGBA phase in external magnetic field[48]. They have reported twist angle between two neighboring smectic A blocks to be $26 \pm 10°$.

A theoretical group at Bristol carried out the simulation study of the TGB phase in 1998[49]. Allen *et al.* in their simulation study imposed a twist in the direction orthogonal to the preferred orientation[49]. On quenching the system from a twisted nematic phase to a state point within the SmA phase, they observe a structure, which corresponds closely to that of TGBA phase.

3. Tilted TGB phases

In 1991, Renn and Lubensky predicted two more TGB phases namely TGBC and TGBC*[50,51]. TGBC and TGBC* would correspond to Abrikosov vortex lattices in a hypothetical superconductor where the Ginzburg parameter (K) is negative and the photon shows Bose condensation. Renn derived

Figure 3: X-ray diffraction pattern of TGBA phase of 10th homolog of nF2BTF01M7[45]. This pattern exhibits 46 spots equispaced along a ring and is the signature of a commensurate TGBA phase. (Courtesy Prof. L. Navailles)

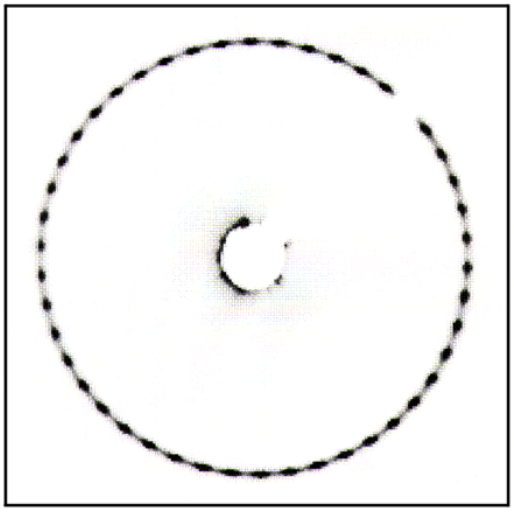

the mean-field phase diagram of the N*-SmA-SmC* within the framework of the chiral Chen-Lubensky model which showed the existence of TGBC and TGBC* phases[51]. Renn predicted that the SmC* can exhibit transitions to the TGBA, TGBC, or TGBC*. In addition he found that both the N*-TGBA and N*-TGBC transitions are possible, but that the N*-TGBC* does not occur[51]. He showed that the TGBA-TGBC transition is replaced by the TGBA-TGBC* transition when the cholesteric pitch length P increases beyond $\sim 2P_C/3$, where P_C is the SmC* pitch length. In the proposed TGBC structure[51], directors of the molecules in the smectic slabs are tilted with respect to the smectic layer normal. In TGBC* phase, slabs are filled by SmC* structure and thus TGBC* has double helix mutually perpendicular to each other. Luk'yanchuk has proposed the TGBC structure in different fashion[52]. He has used TGB_{CP} and TGB_{Ct} notations respectively when smectic layers in the slabs are parallel or tilted to TGB helix axis. X-ray experiments by Navailles *et al.*[53], and the theoretical estimations by Dozov[54] show that TGB_{Ct} structure is indeed more stable. TGB_{Ct} phase has also been called as melted grain boundary (MGB) phase to stress that smectic order parameter vanishes at grain boundaries because of the small distance between screw dislocations[54]. Luk'yanchuk[52] proposed another phase named TGB_{2q} wherein smectic slab is superimposed from two equivalent SmC populations with two smectic layers are inclined to the pitch axis.

The TGBC phase was observed for the first time in the homologous series of 3-fluoro-4-[(R) or (S)-1-methylheptyloxy]-4′-(4″-alkoxy-2″,3″-difluorobenzoyloxy)tolanes ($nF_2BTFO_1M_7$) [53,55,56]. High-resolution calorimetric studies have shown that even two different TGBC phases (namely) TGB_C^{α} and TGB_C^{β} occur for some homologues of $nF_2BTFO_1M_7$series[57]. Two TGBC phases namely TGB_1 and TGB_2 have also been reported in the binary mixtures of 8th and 12th member of nF2BTFO1M7[58]. X-ray studies have shown that the smectic layers are tilted with respect to the helix axis in both of these phases by an angle approximately equal to the SmC director tilt angle[53]. This result differs from the picture originally proposed by Renn and Lubensky[50,51]. The reciprocal lattice consisted either two rings of equispaced Bragg spots or uniform rings confirming the existence of both commensurate and incommensurate TGB phases[53]. The low temperature TGB_1 phase shows a modulation of the X-ray intensity like the commensurate TGBct phase in other systems whereas the high temperature TGB_2 phase seems to be incommensurate. Low temperature TGB_C^{α} phase has also been found to be commensurate TGBct phase[53]. An important point about the structural difference between the predicted and the observed TGBC is the presence of polarization in the later. Dielectric polarization (P_S) has been found to be perpendicular to the pitch axis and varies helically about it[53]. There are several other systems, which show TGBC phase in addition to TGBA phase. A large number of pure systems showing TGBA and TGBC phases have been compiled in a review article on TGB phases[59]. TGBC* phase

Figure 4: The proposed structure of the antiferroelectric twist grain boundary C ($TGBC^*_A$) phase[66].

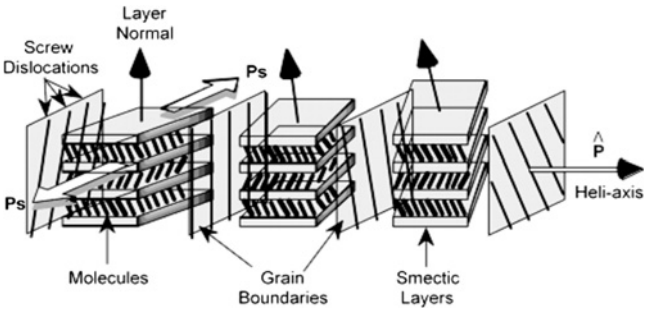

was observed for the first time by Kuczynski and Stegemeyer in the binary mixtures of cholesteryl benzoate and di-heptyloxyazoxybenzene[32,33]. Later TGBC* phase was observed in pure systems as well[21,60]. In 1997, Pramod *et al*, discovered a phase having 2-dimensional undulation of the SmC* like blocks in the form of a square lattice in the binary mixtures of the chiral compound 4-(2′-methyl butyl phenyl 4′-n-octyl biphenyl-4-carboxylate (CE8) and 2-cyano-4-heptyl-phenyl-4′-pentyl-4-biphenyl carboxylate (7CN5)[61]. This phase was not anticipated by the theoretical work of Renn[51]. This phase has been named UTGBC* phase by Pramod *et al.*[61]. Sadashiva realized UTGBC* phase in a single component system[62] and Yelamaggad *et al.* realized it in a trimesogenic system joined together[63]. Pramod *et al.*, proposed a model to explain the UTGBC* phase[61,64]. According to this model SmC* like blocks and the grain boundaries separating them undulate to form a two-dimensional square lattice perpendicular to the TGB helix axis. In a recent article, Brunet *et al.* have proposed a new TGBC/C* structure, based on splayed polarization-twisted director structures adopted by SmC* in planar aligned (bookshelf) geometry[65]. In this work they have explained square/hexagonal grid texture of TGBC* as the superimposed pairs of unwinding lines due to the suppression of the helix within SmC blocks by the grain boundaries (unwinding walls). Fernsler et al have carried out structural analysis of TGBC*/UTGBC* phases showing square grid pattern by freeze-fracture electron microscopy (FFEM), X-ray diffraction (XRD), and depolarized transmission light microscopy[47]. They found that these features arise from a common structure: "giant" smectic blocks of planar layers of thickness $l_b > 200$ nm terminated by grain boundaries that are sharp, mediating large angular jumps in layer orientation between blocks ($60° < \Delta\Psi < 90°$), and lubricating the thermal contraction of the smectic layers within the blocks. They also proposed a theoretical model which is applicable in the limit that the ratio of molecular tilt penetration length-to-layer coherence length is large, and featuring grain boundaries in which smectic ordering is weak, approaching thin, melted (nematic-like) walls. In this limit the energy cost of change of the block size is small, leading to a wide variation of block dimension, depending on preparation conditions. The model also account for the temperature dependence of the TGB helix pitch.

In 2000, Goodby and co-workers discovered another new variants of TGB phase in a compound (S)-1-Methylheptyl 2-[4-(4-dodecyloxybenzoyloxy)phenyl]-pyrimidine-5-carboxylate[66]. On the basis of miscibility, defect textures and electric switching experiment, they have found that this material exhibits antiferroelectric twist grain boundary ($TGBC^*_A$) phase[66–68]. In the proposed structure of $TGBC^*_A$ (see Figure 4), molecules orientation in subsequent layers of smectic slabs changed by approximately 180° resulting formation of antiferroelectric like structure within the slabs. This model has two possible variations, one where the interlayer twist of normal antiferroelectric phase is expelled to the dislocations in the TGB phase, and one where there is a twist perpendicular to the layers and to the in-plane heli-axis of the TGB phase. However, their electrical studies suggest that the polarization vector is probably perpendicular to the in plane twists similar to that in the TGBC phase.

Kamien and Lubensky predicted chiral line liquid (N^*_L) phase between N* and TGBA phases[69]. N^*_L phase is the analog of the flux line liquid occurring in *type II* superconductors with strong fluctuations. Calorimetric studies show that an additional state occurs between N* and TGBA phases[70]. $N^* - N^*_L$ transition is characterized by first order but wide range transition. Initial X-ray structural studies by Navailles *et al.* suggested incommensurate TGBA structure of N^*_L phase[45]. Later high-resolution structural X-ray studies by the

Figure 5: Theoretical phase diagram proposed by Renn[51] including N_L^* phase of Kamien and Lubensky[69]. Theoretical axis $r \sim (T - T_{NAC})$ and $C_\perp$ is the constant appearing in free energy expression (equation 3). The dashed lines represent transitions predicted in the mean field approximation to be second order, and the solid lines are predicted to be first order[51]. The dotted line represents the estimated location of the locus of maxima in the response function for the $N^* - N_L^*$ change in short range order[69]. B1-B3, L and CEP are the multi critical points[51]. In another phase diagram Renn predicted occurrence of TGBC* between TGBC and SmC* (Figure 11 of ref. 50). TGBC-TGBC* transition was also predicted to be second order.

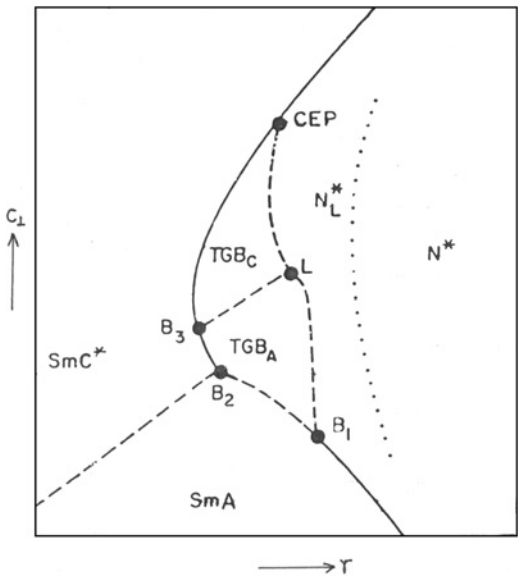

same group determined more precise structure of N_L^* phase[71]. According to which structure of N_L^* phase has been proposed as a liquid of screw dislocations in a SmA matrix, analogous to the liquid of magnetic vortices found in type-II superconductors in between the ordered Abrikosov lattice and the normal conductor phase. Smectic correlation length in this phase has been found to be consistent with the existence of dislocations and hence supporting the theory of Kamien and Lubensky[69].

Mean-field phase diagram for chiral systems within the framework of the chiral Chen-Lubensky model derived by Renn[51] including N_L^* phase predicted by Kamien and Lubensky[69] is shown in Figure 5. This phase diagram predicts the occurrence of the various types of TGB phases in the vicinity of A-N*-C* multicritical point. Such a phase diagram has been experimentally realized in some pure systems[57,70,72] and is shown in Figures 6 and 7. Such a phase diagram has been realised in a binary system composed of 3β-chloro-5-cholestene (ChCl) and 4-n-decyloxybenzoic acid (DOBA)[39].

Discussions of the TGB phases observed in thermotropics will be incomplete if their cousins 'lyotropics' are overlooked. Kamien and Lubensky in 1997 predicted the possibility of TGB and N_L^* phases above lamellar structure[75]. The molecules in lyotropic membranes are typically aligned with the surface normal. When the molecules are chiral, there is a tendency for the molecular direction to twist. These competing effects can reach a compromise by producing helicoidal defects in the membranes. Unlike thermotropic smectics, the centres of these defects are hollow and thus their energy cost comes from the line energy of an exposed lamellar surface[75]. Possible phase diagrams for the lyotropic systems showing TGB and N_L^* phases are shown in Figure 8, however experimental realization has yet not become possible.

4. Characteristics optical textures of TGB phases

Optical texture study under the polarizing microscope is the basic tool to identify liquid crystalline phases. TGB phases are also most often characterized on the basis of their characteristic textures under the different kinds of the anchoring of molecular directors. A very characteristic pattern for TGBA phase is the filament texture shown in Figure 9, which occurs for the anchoring of the director normal to the bounding surfaces of the sample (homeotropic)[76]. If SmA phase occurs in the temperature range below the TGB phase, the

Figure 6: Experimental phase diagram for the chiral series of $nFBTFO_1M_7$, originally reported by Chan *et al*.[70] (after the work of C. W. Garland[72]). Dashed line represents second order transition whereas solid lines represent first order transition. The character of TGBA-TGBC transition could not be ascertained but presumed to be first order.

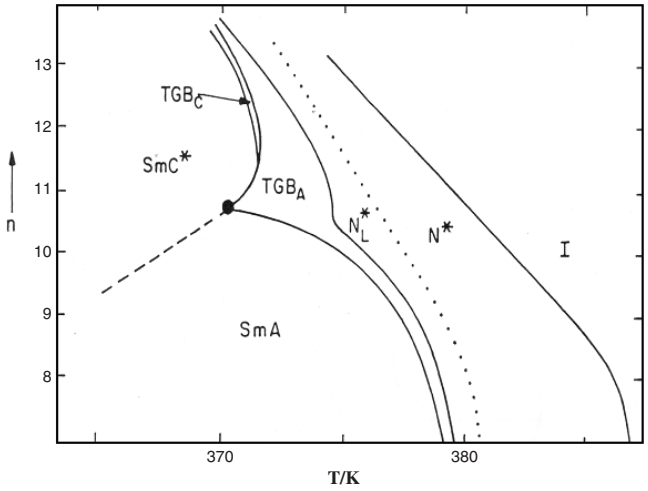

Figure 7: Experimental phase diagram for the chiral series of $nF_2BTFO_1M_7$ with n=9,10,11 and 12 [57]. Dashed line representing $N^* - N_L^*$ transition is the locus of a C_P maximum in the twisted nematic (cholesteric) range (Courtesy Prof. L. Navailles).

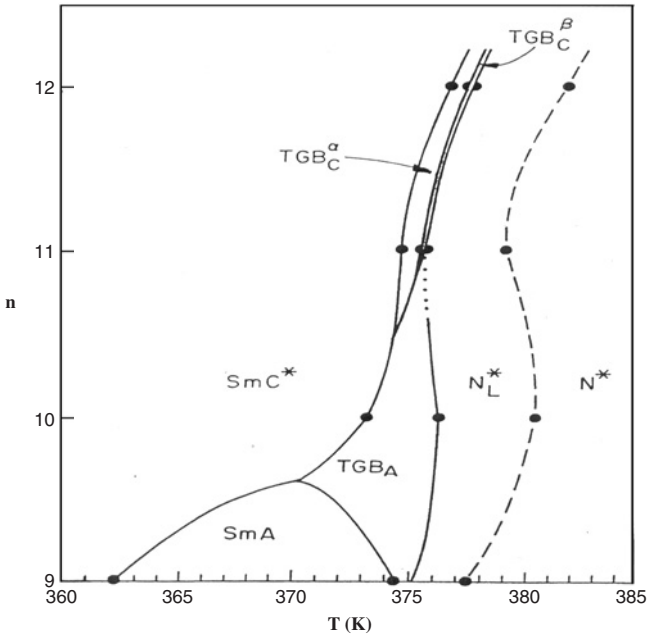

sample appears black between the cross polarizers in the SmA temperature range. On heating from SmA phase, small bright filaments start growing at the SmA-TGBA transition. To distinguish TGBA texture from a cholesteric texture just above SmA phase, requires very careful examination of the two textures. Most often TGBA filaments are curved shaped[32,33,76,77] whereas cholesteric filaments that appear only in a very narrow temperature range close to SmA-N* transition are generally straight. Optical texture shown in Figure 9a is seldom observed however filamentary texture is most

Figure 8: Proposed phase diagram for the lyotropic system as a function of chirality (q_0) and surfactant density (ρ)[75]. Solid lines indicate first order transitions while broken lines indicate second order or weakly first order transitions. (a) Lyotropic with four distinct phases: lamellar, TGB, N_L^* and isotropic. (b) It is possible that the isotropic phase intervenes *before* the TGB phase occurs. The *phantom* (unrealistic) TGB phase region is shown with hatched lines: it will never appear.

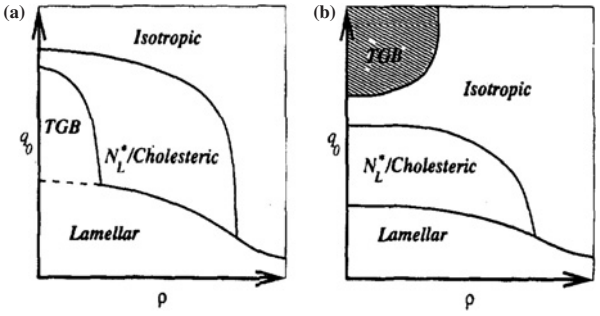

commonly observed for homeotropic aligned TGBA sample (see Figure 9 b). Oily streaks are also formed if two glass plates (containing homeotropically aligned TGBA phase) are slightly sheared or pressed[38,73]. In the case of homeotropic anchoring, helix axis of TGB phase lies parallel to bounding surfaces (as in the case of planar aligned SmC* phase) hence pitch lines some times appear in the form of finger print texture[78]. TGB droplets with a free surface can also show fingerprint texture, which is typical for a helical structure[79].

For parallel anchoring of the director, the TGBA phase resembles to the Grandjean texture of cholesteric phase[80]. If the compound shows an N*-TGBA transition, its only indication is a slight widening and smearing out of the 'oily streaks' which are the characteristics of the N* phase[81]. In wedge shaped cells with parallel anchoring, the TGBA phase shows Grandjean-Cano (GC) lines[56,77] like the cholesteric phase. However, additional defect lines appear between χ-disclinations. TGBC phase also shows textures almost similar to TGBA phase but some time different textures are also observed. TGBC* phase shows square grid pattern (see Figure 10) in planar alignment[32,33,80] and filamentary texture (see Figure-11) in homeotropic alignment[21]. The filaments that are observed in TGBC* phase are different from those in the TGBA and TGBC phases. The TGBC* filaments are undulatory in nature with the period of undulation being about the same as that of the square grid pattern obtained in the planar geometry[21,82]. According to the model of Pramod *et al.*[61], appearance of the square grid structure in TGBC* phase is the consequence of the undulation of the smectic slabs. However according to the model of Galerne[83], which is an extended model of Renn[51], grid structure develops due to the helislabs separated by disclination lines. Optical textures discussed here above are most often but not always observed for TGB phases. Focal conic and many other type of textures have also been observed for TGBA phases[77,84,85]. Peculiar TGB textures can be seen in recent reviews of optical textures of TGB phases by Dierking and Lagerwall[84] and Ribeiro *et al.*[85]. Kleman and coworkers have developed a theoretical approach for the identification of TGBA phase through its defect textures especially with respect to N* texture[86]. This theoretical approach also explains developable domain and cylindrical/marginal cone like textures of TGB phases as reported by Ribeiro *et al.*[85].

Some interesting effects have been observed under the special conditions. The combination of cholesteric and smectic properties, which is apparent in TGB phase, can be clearly seen under the microscopic observation if the confining surfaces of the upper and lower glass plates are treated in order to give different alignments[87]. By applying an electric field, the filaments observed under homeotropic anchoring condition can be aligned in the direction parallel to the field[87]. Square grid pattern of TGBC* phase changes to finger print pattern when a. c. electric field is applied orthogonal to TGB helix[88]. On applying an a. c. electric field exceeding a certain threshold parallel to the helix-axis of the $TGBC_A$ Grandjean texture, the texture changes into a focal conic like texture in thin cells and fingerprint texture in thick cells[78]. Here $TGBC_A$ is the TGBC phase formed in an anti ferro-electric material. TGB texture similar to the columnar phases can be induced at the TGB-isotropic interface by moving the sample along a temperature gradient[89,90]. Such a TGB texture has been attributed to the occurrence of micro columns

Figure 9: (a) Filament texture of TGBA phase of a ferroecene based chiral schiff's base derivative in homeotropic alignment when heated from SmA phase[76] (Courtesy Dr. T. Seshadri). (b)Optical texture of homeotropic aligned sample of the binary mixture of 7OCBand 5*CBB having mole ratio 0.8 and 0.2 in TGBA phase at 36.0 °C when cooled from N* phase[103].

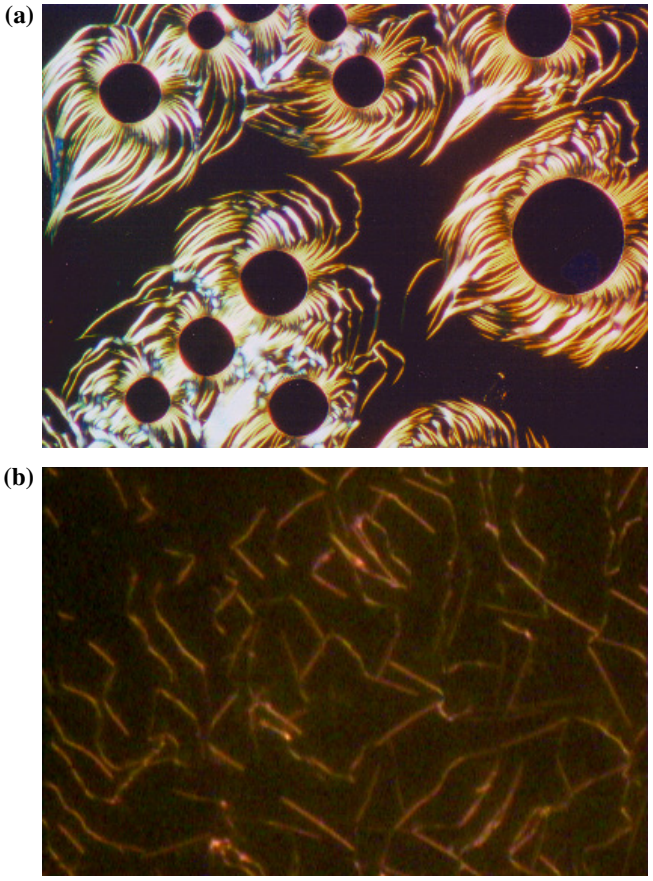

Figure 10: Square grid texture of TGBC* phase observed in ChB-HOAB binary mixture in planar orientation[32] (courtesy Prof. W. Kuczynski).

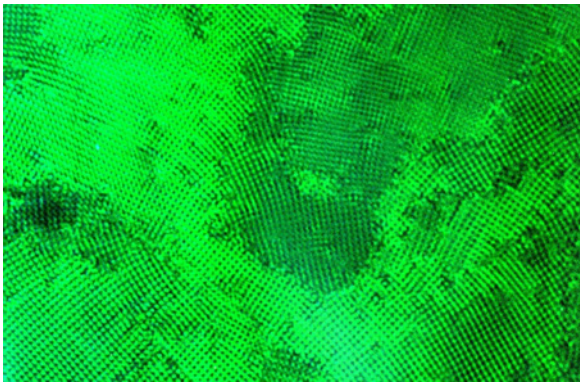

existing in the grain boundary regions[79]. Unaligned samples of TGB phases most often show spiral fan shape texture[24,73,91–93]. Sometimes unaligned samples of mixtures[94] show textures which belong to

Figure 11: Undulated filament texture of TGBC* phase of cholesteryl 6-[4-(4-hexyloxyphenylethynyl) phenoxy] hexanoate in homeotropic alignment (a and b are taken from different regions of the sample[82]. Periodicity of undulation is approximately the same as that of the spacing in square grid pattern observed for planar oriented sample (courtesy Dr. S. Krishna Prasad/Dr. D. S. Shankar Rao).

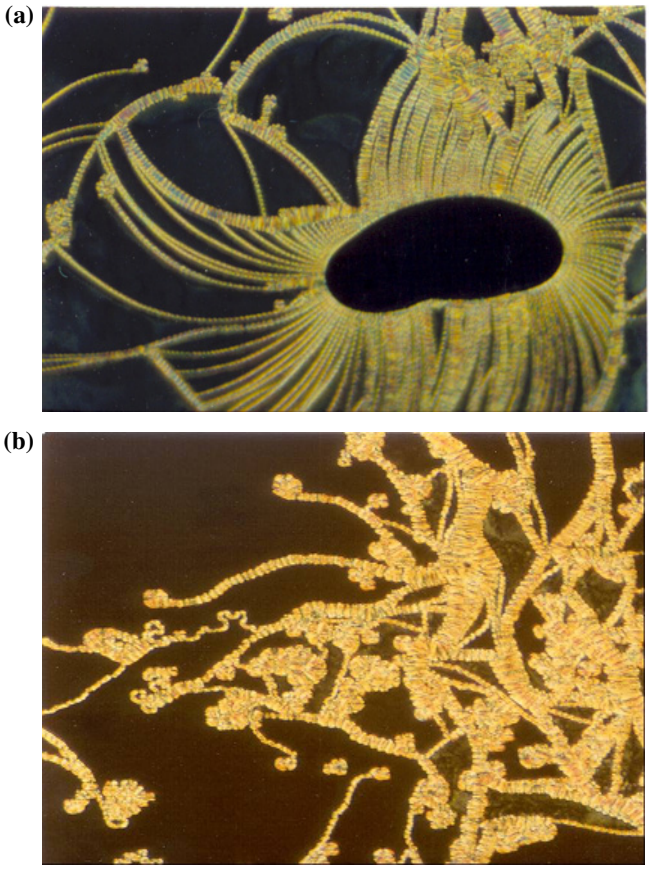

the group of cylindrical/marginal cone like texture recently reported by *Ribeiro et al.*[85] and is some times shown by columnar phases[95].

5. Static dielectric behaviour of TGB phases

Studies on the static and dynamic dielectric properties of TGB phases are scarce[19,39,96–102]. Initial static permittivity studies of TGB phases show that it is difficult to get principal components of permittivity due to alignment problems and small temperature interval of TGB phases. However, Allahabad group has studied and reported static values of permittivity in various mixtures and few pure compounds having wide temperature range of TGB phases[19,39,103–107]. Variations of $\varepsilon'_{\perp}$ and $\varepsilon'_{\parallel}$ (100 Hz) indicating variation of the dielectric anisotropy ($\delta\varepsilon' = \varepsilon'_{\parallel} - \varepsilon'_{\perp}$) with the temperature for a pure compound 4-*n*-undecyloxy-4′- (cholesteryloxycarbonyl-1-butyloxy)chalcone (DC-411) possessing TGBA and TGBC* phases is shown in Figure 12[105]. Keeping in mind that in the case of homeotropic aligned TGB phases, all the molecules are not orthogonal to the electrode surfaces; it may be more illustrative to express measured permittivity data in terms of TGB helix axis. When TGB helix axis is taken as reference axis then $\varepsilon'_{\perp}$ becomes $\varepsilon'_{\parallel h}$ i.e. permittivity measured along TGB helix axis. Similarly, $\varepsilon'_{\parallel}$ becomes $\varepsilon'_{\perp h}$ i.e. permittivity normal to TGB helix axis. As expected, in the isotropic liquid phase, $\delta\varepsilon'$ has been found to be $\cong 0$ showing that there is no preferred alignment of the molecules. Below isotropic liquid to TGBA transition temperature (T_{I-TGBA}), $\varepsilon'_{\perp}$ increases (whereas $\varepsilon'_{\parallel}$ decreases sharply) with decrease in the temperature showing negative dielectric anisotropy ($\delta\varepsilon' < 0$) in the TGBA phase. Good planar alignment has not been achieved immediately below T_{I-TGBA}, but as temperature decreases in TGBA phase, molecular alignment improves and that is why $\varepsilon'_{\perp}$ increases quickly in the vicinity of the isotropic liquid to TGBA transition. After the perfect planar alignment, rate of the increase of $\varepsilon'_{\perp}$ becomes slow

however increasing trend continues throughout the TGBA phase. Dielectric anisotropy shows minimum (~ -1.6) in the TGBA phase at about 118 °C.

It is important to mention here that in the case of TGBA phase, planar oriented molecules are always orthogonal to the measuring electric field irrespective of the rotation of the smectic blocks. Hence measurement of transverse component of the permittivity ($\varepsilon'_\perp$) is usual (similar to that of the normal SmA phase). However, in the case of the cell treated for homeotropic alignment, molecules are not always parallel to the measuring electric field due to rotation of the smectic blocks in the TGBA phase. Hence it is expected that measured value of longitudinal component of the permittivity ($\varepsilon'_\parallel$) is lowered (as compared to virtual normal SmA phase of the same molecular system) due to the twisting of the smectic blocks in TGBA phase. For this reason, values of $\varepsilon'_\parallel$ are unusually low in the TGBA phase. One can say this behaviour unusual, because, average value of the measured dielectric permittivity ($\varepsilon'_{av}=(\varepsilon'_\parallel+2\varepsilon'_\perp)/3$) for the TGBA phase is much lower than the extrapolated average value of the permittivity of the isotropic liquid phase for the TGBA phase.

A clear change in the slope of $\varepsilon'_\perp$ data has been observed at $\sim$110 °C. At TGBA to TGBC* transition, $\varepsilon'_\parallel$ increases very rapidly by appreciable magnitude. Increase in the value of $\varepsilon'_\parallel$ at TGBA to TGBC* transition can be assigned to the tilt of molecules in the smectic blocks. Such a behaviour has been observed in some other similar systems also[104,107]. In the TGBA phase, molecules are always normal to the smectic layers. Hence with the rotation of smectic blocks and hence layer planes (along the TGB helix), molecules are also rotated and no longer normal to the bounding surfaces. In the TGBC* phase, rotating smectic blocks are filled with tilted helical SmC structure in such a way that helix of the SmC* structure is always normal to the TGB helix. Hence it is just possible that molecules of many more TGB blocks (as compared to TGBA phase) are normal to the electrodes surfaces (due to surface anchoring forces) whereas the blocks and hence smectic layers are rotated by about the tilt angle[105]. This causes increase in the longitudinal component of the permittivity ($\varepsilon'_\parallel$) at TGBA to TGBC* transition. This phenomenon also explains better homeotropic alignment of TGBC/C* structure as compared to TGBA by the bounding surfaces treatment technique. However, one should not forget that TGB in general and TGBC* structure in particular are complex one and thus $\delta\varepsilon'$shown in Figure 12 is not directly representing dielectric anisotropy as defined for the simplest nematic and orthogonal smectics.

6. Molecular dynamics of TGB phases

Initial dynamic dielectric studies of the TGBA phase[96–100] show that, like those of SmA* phase, electric field induces amplitude fluctuation of tilt angle and hence soft mode dielectric relaxation is observed in TGBA phase. Similarly in TGBC phase, electric field induces phase fluctuation of the tilt angle and hence Goldstone mode of dielectric relaxation is observed like those in SmC* phase[100]. However experimental evidences suggest that TGB phase relaxation processes have lower amplitudes and higher relaxation frequencies as compared to those observed in classical SmA* and SmC* phases. Ismaili *et al.*[101] have proposed a theoretical model verified by some experimental work as well, which suggests that Goldstone mode of TGBC and soft mode of TGBA phases are strongly reduced due to the existence of an elastic parameter (H_2) in these phases. Ismaili *et al.* obtained the dielectric strengths of the Goldstone mode ($\Delta\varepsilon_G$) and of the soft mode ($\Delta\varepsilon_S$) as[101]

$$\Delta\varepsilon_G = \frac{\varepsilon_0\chi_e^2C^2}{H_2}\cos\theta_S^2 \tag{5}$$

and

$$\Delta\varepsilon_S = \frac{\varepsilon_0\chi_e^2C^2}{\alpha'(T-T_C)+H_2} \tag{6}$$

Relaxation frequencies of the Goldstone mode (f_G) and of the soft mode (f_S) are as follows

$$f_G = \frac{H_2}{2\pi\gamma'_G} \tag{7}$$

and

$$f_S = \frac{\alpha(T-T_C)+H_2}{2\pi\gamma_S} \tag{8}$$

with

$$H_2 = \frac{8\beta_a^2}{1-\beta_a^2/3}\frac{K_{22}}{l_b^2} \tag{9}$$

where θ_S is the spontaneous tilt angle of TGBC phase, C expresses the linear coupling between the tilt and the polarization, $T_C = T_0+\varepsilon_0\chi_eC^2/\alpha$ with T_0 representing SmA-SmC transition temperature in a non-chiral compound. Existence of H_2 is connected to the elastic distortion of the director and its amplitude depends strongly on the anchoring parameter (β_a) arising due to the anchoring forces at the grain boundaries and distance between the grain boundaries (l_b). Variation of relaxation frequency and inverse of dielectric strength of TGBA phase in a compound 9F2BTFO1M7[101] are given in Figure 13 and 14 respectively. In these figures

Figure 12: Variation of $\varepsilon'_{\parallel}$ (triangle) and $\varepsilon'_{\perp}$ (circle) with temperature at 100 Hz showing dielectric anisotropy ($\Delta\varepsilon'$) with the temperature of 4-*n*-undecyloxy-4′-(cholesteryloxycarbonyl-1-butyloxy)chalcone[105].

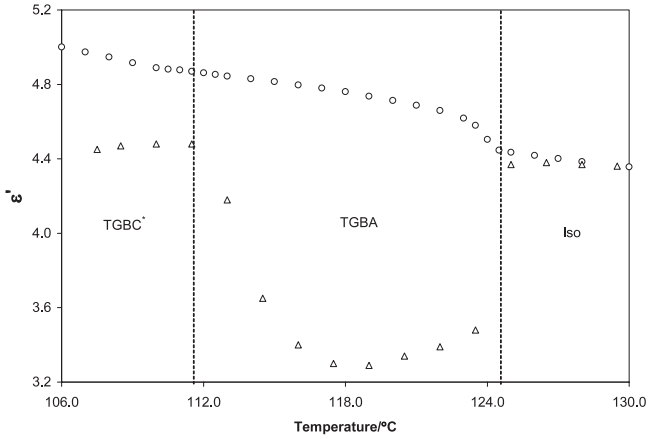

Figure 13: Points and lines: critical frequency versus temperature for the 9F2 *BT*FO1*M*7 compound. Line: extrapolation of the relaxation frequency of the Sm-*A* phase to the TGB*A* phase existence domain[101].

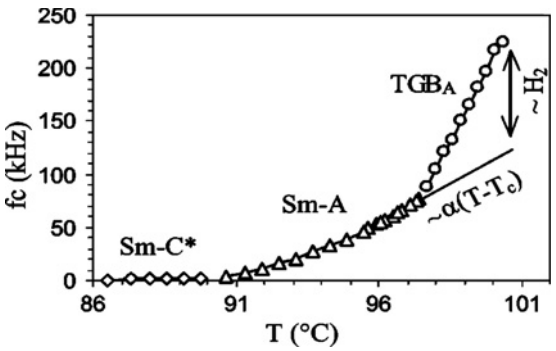

the TGBA-SmA transition is well identified by the slope change of $\Delta\varepsilon^{-1}(T)$ and $fc(T)$. Difference between slopes of TGBA phase and the values extrapolated from the SmA phase directly highlights the existence of the elastic parameters (H_2) in the TGBA phase. Ismaili et al. have also calculated the elastic parameters (H_2) in other homologous of series (namely 11F2BTFO1M7) having TGBC phase[101] by theoretically comparing the slope of SmA phase of the compound 9F2BTFO1M7 (see Figures 15 and 16).

Xu et al have reported effect of bias electric field in the TGBA phase and found that relaxation frequency of the soft mode decreases[99]. Dependence of the soft mode relaxation frequency of TGBA phase on bias voltage is quite opposite to that of the soft mode of SmA* phase. Xu *et al.* have assigned this effect to the unwinding of TGB helix due to the application of bias voltage. Unwinding of TGB helix under planar orientation is rather surprising and needs clear experimental demonstration. Xu *et al.*[99] have reported the existence of another low frequency mode ($\sim$ 1 kHz) beside soft mode at about 100 kHz and assigned it as the relaxation process in grain boundaries. Dielectric spectra of thin cell (1.5 μm) in which TGBA helix is unwound (by the surface of the cell) shows only soft mode relaxation like those of SmA* phase. Application of a high bias voltage across cell has shown occurrence of another relaxation mode due to the deformation process. Dodge et al. have also observed a soft mode relaxation in TGBA and TGBC phase of a compound AH29 (see Figures 17 and 18)[102].

In the antiferroelectric TGBC$^*_A$ phase, a relaxation mode in kHz region has also been

Figure 14: Points and lines: $\Delta\varepsilon^{-1}$ versus temperature for the 9F2 *BT*FO1*M*7 compound. Line: extrapolation of $\Delta\varepsilon^{-1}$ of the Sm-*A* phase to the TGB*A* phase existence domain[101].

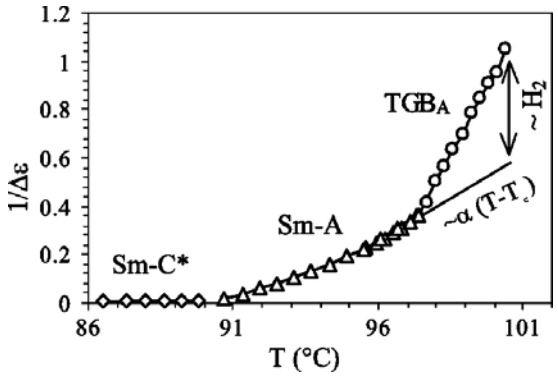

Figure 15: Points and lines: Critical frequency versus temperature for the 11F2 *BT*FO1*M*7 compound. Line: relaxation frequency for the Sm-*A* phase of the 9F2 *BT*FO1*M*7 compound[101].

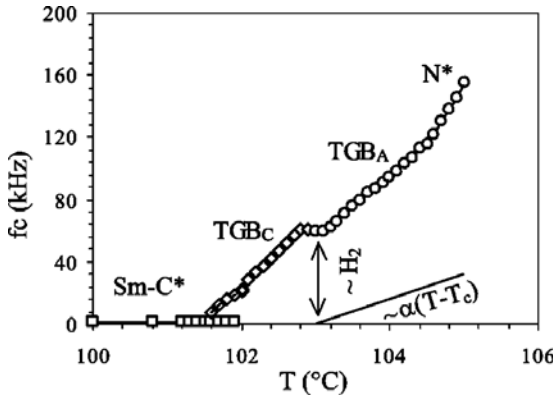

reported by Petrenko et al of (S)-1-Methylheptyl 2-[4-(4-dodecyloxybenzoyloxy)phenyl]-pyrimidine-5-carboxylate [67–68]. Relaxation frequency and corresponding dielectric strength of this mode does not change with temperature. However, this mode is attributed to the soft mode like absorption.

Many of the dielectric studies carried out so far is on narrow temperature range TGBA and TGBC phases shown by ferroelectric liquid crystal materials. We have carried out the frequency dependent dielectric spectroscopy of a wide temperature range TGBA phase ($\sim 31°$C) observed in a binary mixture of 7OCB and 5*CBB with a re-entrant cholesteric phase[103,108]. This mixture, however, does not posses ferroelectric SmC* phase and hence different from previous dielectric spectroscopic studies of TGBA phase. This material is unique in many aspects. Observed TGBA phase is quite different in nature as compared to those previously reported. The known TGB phases exist only above layered SmC or SmA phases and have layers spacing comparable with the molecular length. Here the observed phases are in unique phase sequence: N*-TGBA-N$^*_{re}$ and is chiral analog of N-SmA-N$_{re}$ [109]. TGBA phase exists as the only one smectic phase in broad temperature range. Such situation may occur in mixtures of polar nematic compounds (or polar cholesteric compounds) in which induced partially bilayer smectic phase (A_d phase) arises in the form of an island surrounded by "nematic see". Dabrowski group has reported many of such systems[110] wherein two ring nematic cyano molecules were mixed with three ring cyano molecules. When a member of bicomponent mixture or multicomponent mixture is a chiral compound, the smectic A_d island is surrounded by TGBA phase. There are two ranges of concentration, on right and left hand side of an A_d

Figure 16: Points and lines: $\Delta\varepsilon^{-1}$ versus temperature for the 11F2 *BT*FO1*M*7 compound. Line: $\Delta\varepsilon^{-1}$ for the Sm-*A* phase of the 9F2 *BT*FO1*M*7 compound[101].

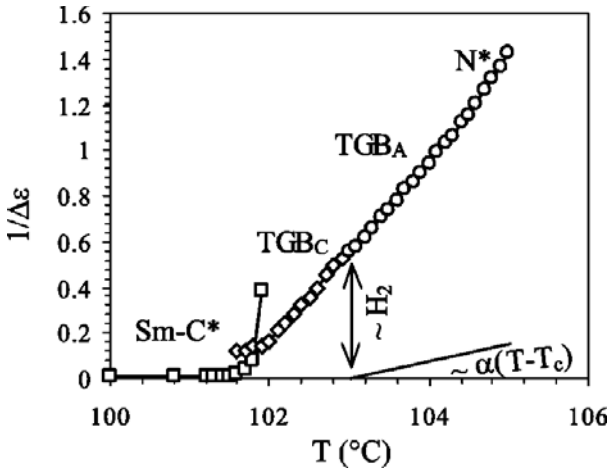

Figure 17: Dielectric loss as a function of temperature and frequency for compound AH29[102].

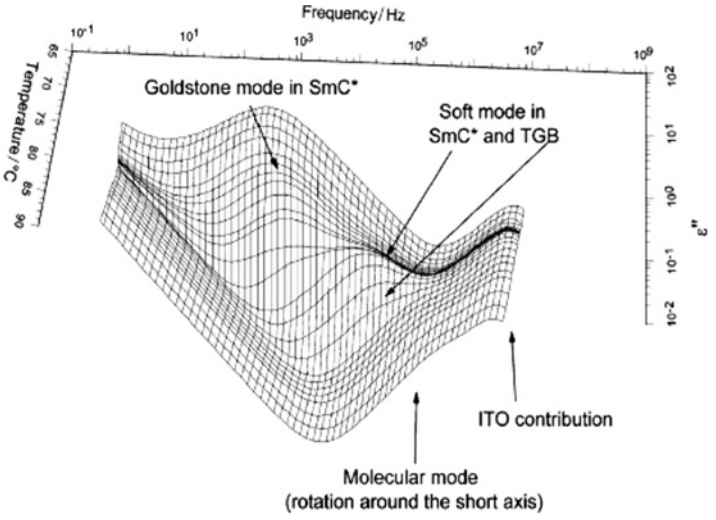

island, where the only induced phase is TGBA phase and this phase has also partially bilayer character. The system with the island consisted of only TBGA phase was also found in reference[110].

Relaxation frequency of a mode observed in the TGBA phase of planar aligned sample of 7OCB and 5*CBB mixture (see mode M1 of Figure 19) lies in the range of 200 kHz–2 MHz[103]. Its dielectric strength ($\Delta\varepsilon$) varies from 0.42 to 0.18 (see Figure 20) while going from lower temperature side (30 °C) to higher temperature side (42 °C). Above 42 °C, it could not be possible to explore the M1 mode of TGBA phase due to its weak dielectric strength and high value of relaxation frequencies. Dielectric strength of the M1 mode follows Curie-Weiss type behaviour as

$$\Delta\varepsilon = \frac{C}{T - T_C} \tag{10}$$

Least square fit of inverse of $\Delta\varepsilon$ with T is straight line (see Figure 20) and it intercepts temperature axis at $T_C = 24.8°$ C, which agrees with TGBA to N^*_{re} transition temperature. On the basis of above characteristics, M1 has been identified as the soft mode of the TGBA phase.

Figure 18: Relaxation frequency of all observed relaxation modes with temperature for compound AH29. The inset is an enlarged version of a 6 °C wide temperature region, which includes isotropic, TGB and SmC* phase[102].

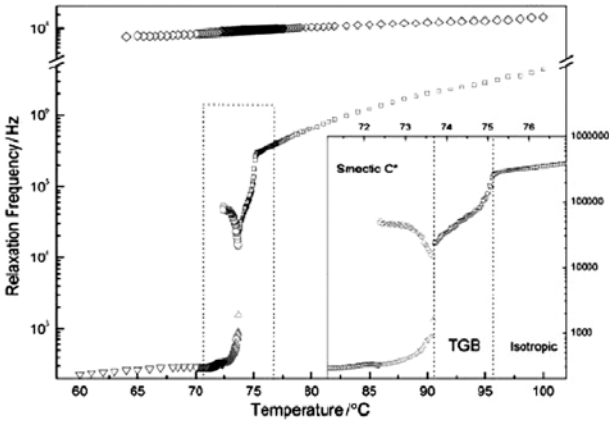

Figure 19: Variation of relaxation frequencies with temperature for the binary mixture of 7OCB and 5*CBB having mole ratio 0.8 and 0.2[103]. M1 has characteristics similar to that of the soft mode relaxation of TGBA phase observed in the planar aligned sample whereas M2 represents dielectric relaxation corresponding to the individual molecular rotation about their short axes observed in homeotropic aligned sample. Existence of M1 below TGBA-N^*_{re} transition seems consequence of wide range of the transition process.

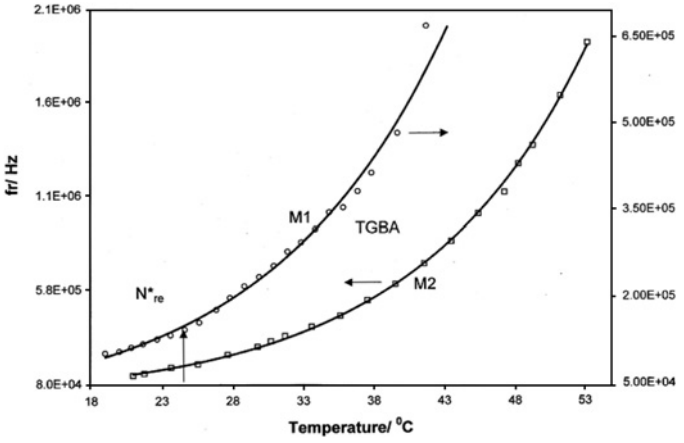

Recently, we have carried out frequency dependent dielectric studies of 4-*n*-undecyloxy-4′-(cholesteryloxycarbonyl-1-butyloxy)chalcone (DC-411)[105,106] and 4-*n*-decyloxy-4′-(cholesteryloxycarbonyl-1-butyloxy) chalcone (DC-410)[107] having wide temperature range TGBC* phase below TGBA phase. These materials show the existence of two collective modes in the TGBC* phase at low and high frequency range respectively[105,106]. Dielectric permittivity in planar configuration ($\varepsilon'_\perp$) of DC-411 with temperature at various frequencies is shown in Figure 21. $\varepsilon'_\perp$ is almost constant in the frequency range of 100 Hz to 1 MHz for all the temperatures of the isotropic liquid phase implying that no molecular relaxation exists in this phase. At the isotropic liquid to TGBA transition, $\varepsilon'_\perp$ increases rapidly (see Figure. 21). On lowering the temperature in the TGBA phase below ~ 119 °C, it has been found that $\varepsilon'_\perp$ is no more constant in the frequency range of 100 Hz–1 MHz. $\varepsilon'_\perp$ shows some decrease for the frequencies above 100 kHz, indicating a pre dielectric dispersion phenomenon in the frequency range of 100 kHz–1 MHz (see Figure 21). As temperature goes down,

Figure 20: Variation of dielectric strength ($\delta\varepsilon$) and inverse of the dielectric strength $(\delta\varepsilon)^{-1}$ for the soft mode of TGBA phase[103]. Vertical broken line represents TGBA-N^*_{re} transition temperature of the sample. Straight line obtained by least square fit of $(\delta\varepsilon)^{-1}$ with temperature T (shown by solid straight line) intercepts temperature axis at 24.8 °C which is almost TGBA-N^*_{re} transition temperature.

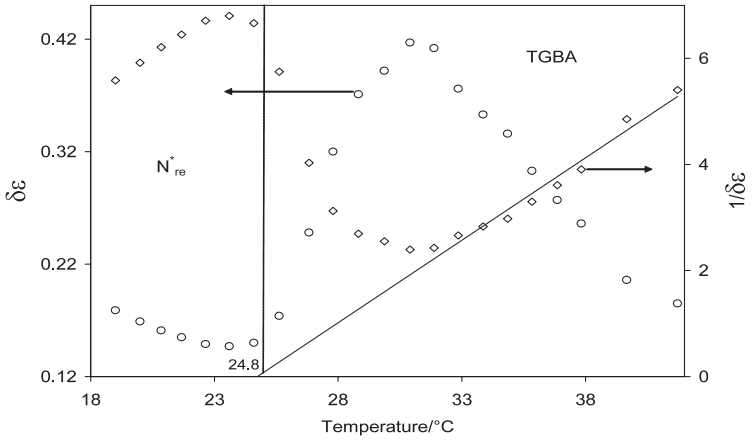

Figure 21: Variation of $\varepsilon'_\perp$ with temperature at 100 Hz (square), 1 kHz (cross), 10 kHz (triangle), 100 kHz (circle) and 1 MHz (plus) of 4-*n*-undecyloxy-4′-(cholesteryloxycarbonyl-1-butyloxy)chalcone[105]. Broken vertical lines represent transition temperatures on the basis of the combined (thermodynamic, optical texture and dielectric) studies.

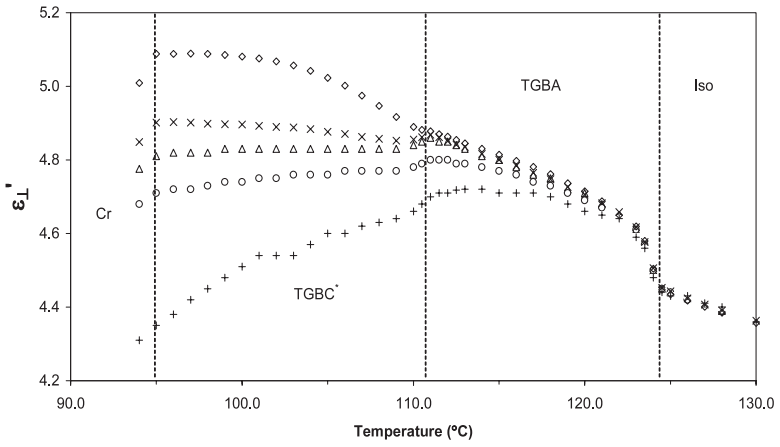

this mechanism further dominates. From figure 21, one can see that, while going from 10 kHz–1 MHz, $\varepsilon'_\perp$ decreases by ~0.2 (at 111 °C). This indicates that dielectric strength of the expected relaxation mode is very weak. In principle, one may expect soft mode relaxation in TGBA phase under planar anchoring of the molecules[102]. On the basis of the range of the relaxation frequency and its strength, this weak relaxation mode has been assigned to soft mode of TGBA phase[105]. At TGBA-TGBC* transition, low frequency values (10 Hz–100 Hz) of $\varepsilon'_\perp$ further go up however high frequency values of $\varepsilon'_\perp$ move down (see Figure 21). It is apparent from these dielectric data that soft mode of TGBA phase continues in TGBC* phase as well, with increase in its strength. In the low frequency region (<1 kHz) of TGBC* phase, $\varepsilon'_\perp$ increases upon decreasing temperature. This indicates the presence of another collective relaxation mechanism in TGBC* phase between 1 kHz–10 Hz; however data below 100 Hz are affected due to low frequency parasitic contributions (see Figure 22). The measured data have been fitted

Figure 22: Variation of $\varepsilon'_{\perp}$ with frequency (a) for DC-411[105] at 96°C, 100°C, 104°C and 108°C (b) for DC-410[107] in the TGBC* phase to demonstrate a soft mode (on the higher frequency side) and a Goldstone like mode (on the lower frequency side).

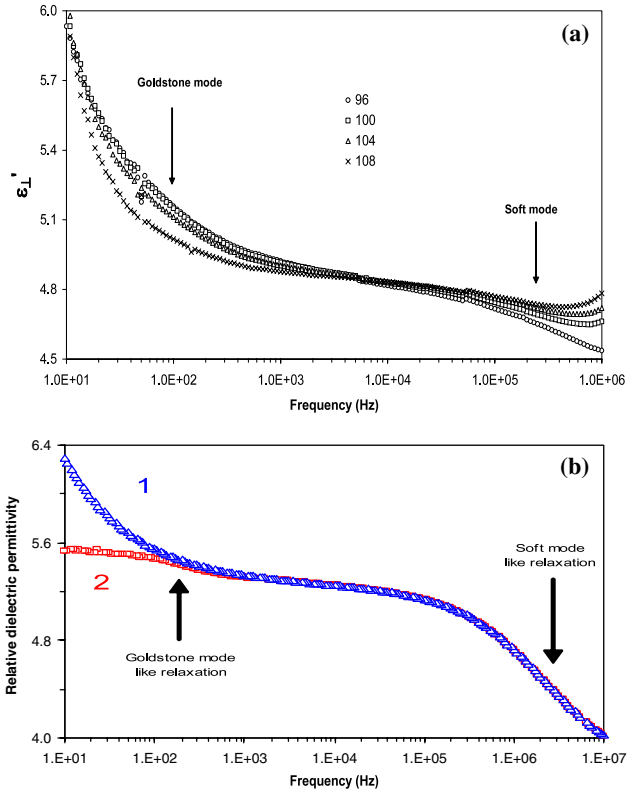

with the help of generalised Cole-Cole equation. After subtracting the low frequency artifacts due to electrode polarization from measured data, a mode below 1 kHz is clearly visible at all temperatures of TGBC* phase. Goldstone and soft modes of TGBC* phase are more clear in the material DC-410[107] (see Figure 22b). The variations of relaxation frequency and dielectric strength with temperature for the Goldstone mode of TGBC* phase are shown in Figure 23. It has been found that relaxation frequency decreases whereas the dielectric strength increases continuously with decrease in temperature. Small value of the transverse component of the molecular dipole moment may be another reason for the weak dielectric strength of the observed mode in TGB systems. Novotna et al. have reported soft and Goldstone mode in TGBA and TGBC* phase of a series HZLn/*[111]. Softening behaviour has been reported for the observed mode of TGBA phase in all studied compound of the series. For this material, the strength of the Goldstone mode of TGBC* phase is found to be large (~100) and relaxation frequency shows strong temperature dependence which was not typical for Goldstone mode of SmC* phase[111]. We may stress that any firm evidence has not been found to relate observed modes of TGB systems to tilt and phase angle fluctuations; nevertheless this hypothesis still remain the most likely explanation. However, a most interesting system yet to be explored for rich varieties of dielectric relaxation modes would be one having phase sequence: N*-TGBA-TGBC-TGBC*-SmC* with large value of the normal component of dielectric permittivity.

7. Concluding remarks

Discovery of TGB phase has opened new vistas of research activities in the field of liquid crystals. Extensive studies on TGB phases during the last two decades have proven it a very exciting new field of research. Many of the predicted TGB phases have been experimentally realized; however in spite of the many similarities between theoretical predictions and experimental observations, there are several issues that need more attention. Despite large number of the research papers on TGB phases during last 20 years, most of these are on the synthesis and characterization. Whereas

Figure 23: Variations of relaxation frequency and dielectric strength of Goldstone like mode with temperature in TGBC* phase of (a) DC-411 (ref 106) and (b) DC-410 (ref 107).

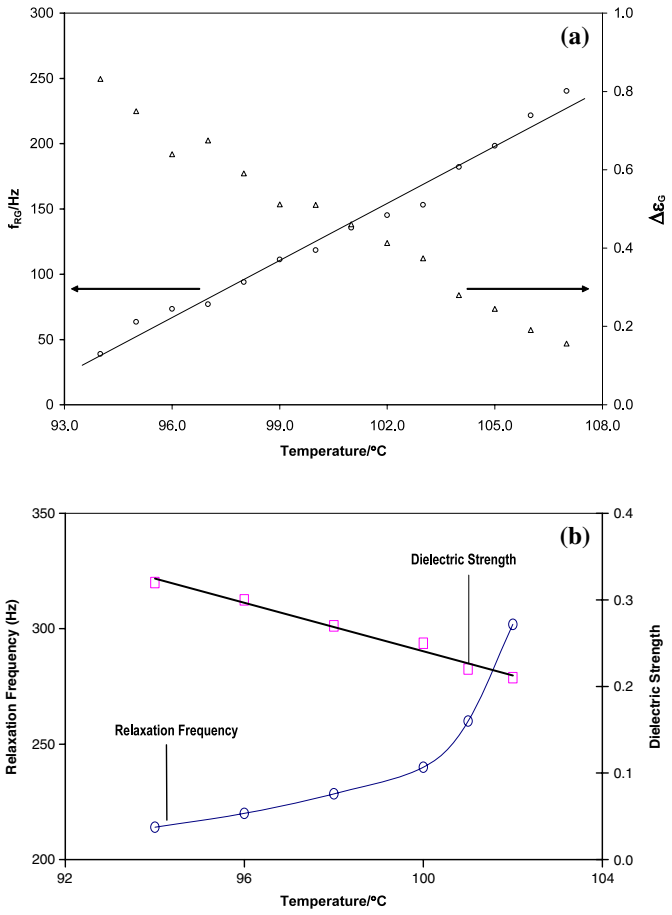

the understanding of the physical properties of these mysterious phases are challenging for both experimentalists and theorists, and many problems are still to be solved. One foremost problem is to see whether TGB phases can be exploited technologically whether directly or indirectly.

8. Acknowledgements

We thank many of the research workers who provided their original optical textures. Thanks to Prof. W. Kuczynski and Dr. S. Krishna Prasad for several discussions on TGB phases. We acknowledge financial support from the University Grants Commission (UGC) and Department of Science and Technology (DST), New Delhi for our work on the above topic. One of us (RD) thanks UGC, New Delhi especially for the National Research Award and thus relieving from the responsibilities other than the research. MBP thanks DST, New Delhi for Young Scientist Project Award and fellowship under the scheme.

Received 22 April 2009.

References

1. G. W. Gray. Molecular Structure and Properties of Liquid Crystals (Academic Press, New York, 1962).
2. P. G. de Gennes, The Physics of Liquid Crystals (Oxford University Press, Oxford, 1975), and P. G. de Gennes and J. Prost, 2nd ed. (Oxford Science, Clarendon Press, Oxford 1993).
3. S. Chandrasekhar, Liquid Crystals, (Cambridge University Press, Cambridge, 1st ed. 1977, 2nd ed.1992).
4. P. J. Collings and M. Hird. *Introduction to Liquid Crystals: Chemistry and Physics* (Taylor & Francis, London, 1997).
5. F. Reinitzer, *Wiener Monatsh. Chem.*, **9**, 412 (1888).
6. P. G. de Gennes, *Solid State Commun.*, **10**, 753 (1972).
7. P. G. de Gennes, *Mol. Cryst. Liq. Cryst.*, **21**, 49 (1973).
8. S. R. Renn, and T. C. Lubensky, *Phys. Rev. A*, **38**, 2132–2147 (1988).
9. P. G. de Gennes, *Mol. Cryst. Liq. Cryst.*, **12**, 193 (1971).
10. L. Landau. *Phys Z. Sowjet*, **11**, 545–555 (1937).
11. Ginzburg and L. D. Landau, *Zh. Eksp.Teor. Fiz.*, **20**, 1044 (1950).
12. P. G. de Gennes. Superconductivity of Metals and Alloys, (Benzamin W. A., New York 1966).
13. D. R. Tilley and J. Tilley. Superfludity and Superconductivity (Van Nostrand Reinhold, New York, 1974).

14. W. Buckel, Supraleitung-Grundlagen and Anwendungen, 5th ed., VCH Weinheim (1993).
15. J. W. Goodby, M. A. Waugh, S. M. Stein, E. Chin, R. Pindak and J. S. Patel, *Nature*, **337**, 449–452 (1989).
16. G. Srajer, R. Pindak, M. A. Waugh, J. W. Goodby and J. S. Patel, *Phys. Rev. Lett.*, **64**, 1545–1548 (1990).
17. O. D. Lavrentovich, Y. A. Nastishin, V. I. Kulishov, Y. S. Narkevich and A. S. Tolochko, *Europhys. Lett.*, **13**, 313–318 (1990).
18. S. L. Srivastava, R. Dhar and A. Mukherjee, *Mol. Cryst. Liq. Cryst.*, **287**, 139–154 (1996).
19. S. L. Srivastava and R. Dhar, *Mol. Cryst. Liq. Cryst.*, **317**, 23–36 (1998).
20. V. Vill, H.-W. Tunger and D. Peters, *Liq. Cryst.*, **20**, 547–552 (1996).
21. D. S. Shankar Rao, S. K. Prasad, V. N. Raja, C. V. Yelamaggad and S. A. Nagamani, *Phys. Rev. Lett.*, **87**, 085504(1–4) (2001).
22. S. K. Prasad, G. G. Nair, S. Chandrasekhar, and J. W. Goodby, *Mol. Cryst. Liq. Cryst.*, **260**, 387–394 (1995).
23. R. A. Lewthwaite, J. W. Goodby and K. J. Toyne, *Liq. Cryst.*, **16**,299–313 (1994).
24. J. H. Chen, R. C. Chang, G. H. Hsiue, F. W. Guu and S. L. Wu, *Liq. Cryst.*, **18**, 291–301 (1995).
25. M. Young, G. Pitsi, M. H. Li, H. T. Nguyen, P. Jamee, G. Sigaud and J. Thoen, *Liq. Cryst.*, **25**, 387–391 (1998).
26. R. Shao, J. Pang, N. A. Clark, J. A. Rego and D. M. Walba, *Ferrolectrics*, **147**, 255–262 (1993).
27. M. Werth, H. T. Nguyen, C. Destrade and N. Isaert, *Liq. Cryst.*, **17**, 863–877 (1994).
28. I. Dierking, F. Giesselmann, J. Kusserow and P. Zugenmaier, *Liq. Cryst.*, **17**, 243–261 (1994).
29. B. D. Terris, R. J. Twieg, C. Nguyen, G. Sigaud and H. T. Nguyen, *Europhys. Lett.*, **19**,85–90 (1992).
30. A. S. Petrenko, M. Hird, R. A. Lewis, J. G. Meier, J. C. Jones and J. W. Goodby, *J. Phys.: Condens. Matter*, **12**, 8577–8593 (2000).
31. X. Dai, H. Goto and K. Akagi, *Mol. Cryst. Liq. Cryst.*, **365**, 347–354 (2001).
32. W. Kuczynski and H. Stegemeyer, *Ber. Bunsenges. Phys. Chem.*, **98**, 1322–1324 (1994); W. Kuczynski and H. Stegemeyer, *Mol. Cryst. Liq. Cryst.*, **260**, 377–386 (1995).
33. W. Kuczynski and H. Stegemeyer, *SPIE*, **3318**, 90–93 (1997).
34. Y. Sah, *Mol. Cryst. Liq. Cryst.,* **302**, 207 (1997).
35. J. Mahadeva, Nagappa, K. R. Prasad and P. R. Alapati, *Mol. Cryst. Liq. Cryst.,* **365**, 827–834 (2001).
36. I. Nishiyama, J. Yamamoto, H. Yokoyama, J. W. Goodby, *Mol. Cryst. Liq. Cryst.*, **400**, 21–29 (2003).
37. S. L. Srivastava, and R. Dhar, *Mol. Cryst. Liq. Cryst.*, **366**, 79–90 (2001).
38. R. Dhar, A. K. Srivastava and V. K. Agrawal, *Ind. J. Pure Appl. Phys.*, **40**, 694–700 (2002).
39. R. Dhar, M. B. Pandey and V. K. Agrawal, *Phase Transitions*, **76**, 763–780 (2003).
40. J. W. Goodby, I. Nishiyama, A. J. Slaney, C. J. Booth and K. J. Toyne, *Liq. Cryst.*, **14**, 37–66 (1993).
41. J. W. Goodby, A. J. Slaney, C. J. Booth, I. Nishiyama, J. D. Vuijk, Styring and K. J. Toyne, *Mol. Cryst. Liq. Cryst.*, **243**, 231–298 (1994).
42. J. W. Goodby. Twist Grain Boundary (TGB) Phases. In D. M. P. Mingos (ed.), *Liquid Crystals II*, **95**, Springer-Verlag, Berlin, 83–147 (1999).
43. K. J. Ihn, A. N. Zasadzinski, R. Pindak, A. J. Slaney and J Goodby, *Science*, **258**, 275–278 (1992).
44. L. Navailles, P. Barois and H. T. Nguyen, *Phys. Rev. Lett.*, **71**, 545–548 (1993).
45. L. Navailles, B. Pansu, L. Gorre-Talini and H. T. Nguyen, *Phys. Rev. Lett.*, **81**, 4168–4171 (1998).
46. I. Bluestein, D. Kamien and T. C. Lubensky, *Phys. Rev. E*, **63**, 061702(1–11) (2001).
47. J. Fernsler, L. Hough, R.-F. Shao, J.E. Maclennan, L. Navailles, M. Brunet, N.V. Madhusudana, O. Mondain-Monval, C. Boyer, J. Zasadzinski, J.A. Rego, D.M. Walba and N.A. Clark, Proc. Nat. Acad. Sci. **102**, 14191 (2005).
48. J. Zhang, V. Domenici, C. A. Veracini and R. Y. Dong, J. Phys Chem B, **110**, 15193 (2006).
49. M. P. Allen, M. A. Warren and M. R.Wilson, *Phys. Rev. E*, **57**, 5585–5596 (1998).
50. S. R. Renn and T. C. Lubensky, *Mol. Cryst. Liq. Cryst.*, **209**, 349–355 (1991).
51. S. R. Renn, *Phys. Rev. A*, **45**, 953–973 (1992).
52. I. Luk'yanchuk, *Phys. Rev. E*, **57**,574–581 (1998).
53. L. Navailles, R. Pindak, Barois and H. T. Nguyen, *Phys. Rev. Lett.*, **74**, 5224–5227 (1995).
54. I. Dozov, *Phys. Rev. Lett.*, **74**, 4245 (1995).
55. H. T. Nguyen, A. Bouchta, L. Navailles, P. Barois, N. Isaert, R. J. Twieg, A. Maaroufi and C. Destrade, *J. Phys. Fr. II*, **2**,1889–1906 (1992).
56. N. Isaert, L. Navailles, P. Barois and H. T. Nguyen, *J Phys. II France*, **4**, 1501–1518 (1994).
57. L. Navailles, C. W. Garland and H. T. Nguyen, *J Phys. II France*, **6**, 1243–1258 (1996).
58. L. Navailles, H. T. Nguyen, P. Barois, N. Isaert and P. Delord, *Liq. Cryst.*, **20**, 653–664 (1996).
59. H. S. Kitzerow. Twist Grain Boundary Phases. In H. S. Kitzerow and C Bahr (eds.), *Chirality in Liquid Crystals*, (Springer-Verlag, Berlin, 2001), pp 296–354.
60. C. V. Yelamaggad, M. Mathews, *Liq. Cryst.*, **30**, 125–133 (2003).
61. P. A. Pramod, R. Pratibha and N. V. Madhusudana, *Current Science*, **73**, 761–765 (1997).
62. B. K. Sadashiva, *Pramana*, **53**, 213–222 (1999).
63. C. V. Yelamaggad, S. A. Nagmani, U. S. Hiremath, D. S. Shankar Rao and S. K. Prasad, *Liq. Cryst.*, **28**, 1581–1583 (2001).
64. P. A. Pramod, Y. Hatwalne and N. V. Madhusudana, *Liq. Cryst.*, **28**, 525–533 (2001).
65. M. Brunet, M. L. Navailles and N. A. Clark, *Euro Phys J E*, **7**, 5–11 (2002).
66. J. W. Goodby, A. Petrenko, M. Hird, R. A. Lewis, J. Meier and J. C. Jones, Chem Comm, 1149–1150 (2000).
67. A. S. Petrenko, M. Hird, R. A. Lewis, J. Meier, J. C. Jones and J. W. Goodby, J. Phys.: Condens. Matter, **12**, 8577–8593 (2000).
68. J. G. Meier, P. Rudquist, A. S. Petrenko, J. W. Goodby and S. T. Lagerwall, Liq. Cryst., **29**, 179–189 (2002).
69. R. D. Kamien and T. C. Lubensky, *J. Phys. I France*, **3**, 2131–2138 (1993).
70. T. Chan, C. W. Garland and H. T. Nguyen, *Phys. Rev. E*, **52**, 5000–5003 (1995).
71. C. Ybert, L. Navailles, B. Pansu, F. Rieutord, H. T. Nguyen and P. Barois, *Europhys. Lett.*, **63**, 840 (2003).
72. C. W. Garland, *Liq. Cryst.*, **26**, 669–677 (1999).
73. R. Dhar, A. K. Srivastava and V. K. Agrawal, *Phase Transitions*, **76**, 959–974 (2003).
74. S. I. Torogova, M. P. Petrov and A. Strigazzi, Liq. Cryst., 28, 1439–1449 (2001).
75. R. D. Kamien and T. C. Lubensky. *J. Phys. II France*, **7**, 157–163, (1997).
76. T. Seshadri and H. J. Haupt, *Chem. Commun.*, **1998**, 735–736 (1998).
77. C. D. Cruz, J. C. Rouillon, J. P. Marcerou, N. Isaert and H. T. Nguyen, *Liq. Cryst.*, **28**, 125–137 (2001).
78. J. G. Meier, P. Rudquist, A. S. Petrenko, J. W. Goodby and S. T. Lagerwall, *Liq. Cryst.*, **29**, 179–189 (2002).
79. I. Dierking, Giesselmann and P. Zugenmaier, *Liq. Cryst.*, **17**,17–22 (1994).
80. I. Dierking, *Liq. Cryst.*, **28**, 165–170 (2001).
81. W. Kuczynski. Self Organization in chiral liquid crystals (Scientiffic publishers OWN, Poznan, 1997).
82. C. V. Yelamaggad, U. S. Hiremath, D. S. Shankar Rao, S. Krishna Prasad, *Chem. Commun.*, **2000**, 57–58 (2000).

83. Y. Galerne, *J. Phys. France II*, **4**, 1699–1711 (1994).
84. I. Dierking and S. T. Lagerwall, *Liq. Cryst.*, **26**, 83–95 (1999).
85. A. C. Ribeiro, H. T. Nguyen, Galerne and D. Guillon, *Liq. Cryst.*, **27**, 27–34 (2000).
86. Y. A. Nastishin, M. Kleman, J. Malthete and H. T. Nguyen, *Eur. Phys. J. E.*, **5**, 353–357 (2001); M. Kleman, Y. A. Nastishin and J. Malthete, *Eur. Phys. J. E.*, **8**, 67–78 (2002).
87. J. S. Patel, S. D. Lee, S. W. Suh and J. W. Goodby, *Liq. Cryst.*, **13**, 313–317 (1993).
88. G. G. Nair, S. K. Prasad and C. V. Yelamaggad, *Ferroelectrics*, **277**, 117–124 (2002).
89. P. E. Cladis, A. J. Slaney, J. W. Goodby and H. R. Brand, *Phys. Rev. Lett.*, **72**, 226–229 (1994).
90. A. C. Ribeiro, A. Dreyer, L. Oswald, J. F. Nicoud, A. Soldera, D. Guillon and Y. Galerne, *J. Phys. France II*, **4**, 407–412 (1994).
91. S. L. Wu, and W. J. Hsieh, *Liq. Cryst.*, **21**, 783–790 (1996).
92. C. S. Hsu, and C. H. Tsai, *Liq. Cryst.*, **22**, 669–677 (1997).
93. H. Narihiro, X. Dai, H. Goto and K. Akagi, *Mol. Cryst. Liq. Cryst.,* **365**, 363–371 (2001).
94. R. Dhar, M. B. Pandey and V. K. Agrawal, *Mol. Cryst. Liq. Cryst.*, **409**, 269–284 (2004).
95. J. Malthete, J. Jacques, H. T. Nguyen and C. Destrade, *Nature*, **298**, 46–47 (1982).
96. C. Girold, C. Legrand, N. Isaert, P. Pochat, J. P. Parneix, H. T. Nguyen and C. Destrade, *Ferroelectrics*, **147**, 171–179 (1993).
97. H. T. Nguyen, C. Destrade, J. P. Parneix, P. Pochat, N. Isaert, and C. Girold, *Ferroelectrics*, **147**, 181–191 (1993).
98. S. Wrobel, S. Hiller, M. Pfeiffer, M. Marzec and W. Haase. *Liq. Cryst.*, 18, 21 (1995).
99. H. Xu, Y. P. Panarin, J. K. Vij, A. J. Seed, M. Hird and J. W. Goodby, *J. Phys.: Cond. Matter*, **7**, 7443–7452 (1995).
100. F. Bougrioua, N. Isaert, C. Legrand, A. Bouchta, P. Barois and H. T. Nguyen. *Ferroelectrics*, **180**, 35 (1996).
101. M. Ismaili, F. Bougrioua, N. Isaert, C. Legrand, and H. T. Nguyen, *Phys. Rev. E*, **65**,011701–15 (2001).
102. M. R. Dodge, J. K. Vij, S. J. Cowling, A. W. Hall and J. W. Goodby, *Liq. Cryst.*, **32**, 1045 (2005).
103. M. Gupta, R. Dhar, V. K. Agrawal, R. Dabrowski and M. Tykarska, *Phys. Rev. E*, **72,** 021703 (2005); R. Dhar, *Phase Transit.*, **79**, 175–199 (2006).
104. M. B Pandey, R. Dhar and W. Kuczynski, *Ferroelectrics*, **343**, 69–82 (2006).
105. M. B. Pandey, R. Dhar, C. V. Yelamaggad and A. S. Achalkumar, *J. Phys. Condens. Matter*, **19**, 436219 (2007).
106. M. B. Pandey, R. Dhar, C. V. Yelamaggad and A. S. Achalkumar, *Phase Transitions*, **81**, 449–458 (2008).
107. A. S. Pandey, R. Dhar, M. B. Pandey, C. V. Yelmaggad and A. S. Achalkumar, *Liq. Cryst.* **36**, 13–19 (2009).
108. M. Brodzik and R. Dabrowski, *Liq. Cryst.*, **20**, 99–103 (1996).
109. R. Nozaki, T. K. Bose and S. Yagihara, *Phys. Rev. A*, **46**, 7733 (1992).
110. M. Brodzik and R. Dabrowski, *Mol. Cryst. Liq. Cryst.*, **260**, 361 (1995).
111. V. Novotna, M. Kaspar,V. Hamplova, M. Glogarova, P. Bilkova,V. Domenici and D. Pociecha, *Liquid Crystals,* **35**, 287 (2008).

Dr. Ravindra Dhar received his D. Phil in Science from the University of Allahabad (India) in 1996. He is Associate Professor of Physics at Ewing Christian College, University of Allahabad Allahabad. Currently he is working as University Grants Commission (UGC) National Research Awardee at University of Allahabad. His primary research interest is focused on induced phases in Liquid Crystal Mixtures, Twist Grain Boundary Phases, Ferro- and Anti Ferro-electric phases, Carbon Nanotubes dispersed in Liquid Crystals and Radiation induced transformations in Liquid Crystals. He has published more than 50 research papers in these areas. Currently he is also the member of the editorial board of "Phase Transitions" a multinational journal from Taylor and Francis.

Dr. Manoj Bhushan Pandey received his M. Sc (Physics) from the Banaras Hindu University, Varanasi in 2000 and D Phil in Science from University of Allahabad in 2005. At present, he is Young Scientist Fellow of Department of Science and Technology (DST), Government of India, New Delhi and working at University of Allahabad. His current research activity is focused on dielectric properties of Twist Grain Boundary Phases, Antiferroelectric Liquid Crystals and Chiral Smectic C sub phases (SmC^*_α, SmC^*_β and SmC^*_γ).